A general approach to low noise readout of terahertz imaging arrays

Jonathan D. Chisum, Erich N. Grossman, and Zoya Popovi

Articles you may be interested in

Investigation and optimization of low-frequency noise performance in readout electronics of dc superconducting quantum interference device
Rev. Sci. Instrum. **85**, 054707 (2014); 10.1063/1.4878342

Uncooled antenna-coupled terahertz detectors with 22s response time based on BiSb/Sb thermocouples
Appl. Phys. Lett. **102**, 121102 (2013); 10.1063/1.4798369

Terahertz wavefront measurement with a Hartmann sensor
Appl. Phys. Lett. **101**, 031103 (2012); 10.1063/1.4737164

A readout for large arrays of microwave kinetic inductance detectors
Rev. Sci. Instrum. **83**, 044702 (2012); 10.1063/1.3700812

Frequency-domain multiplexed readout of transition-edge sensor arrays with a superconducting quantum interference device
Appl. Phys. Lett. **86**, 112511 (2005); 10.1063/1.1884746

A general approach to low noise readout of terahertz imaging arrays

Jonathan D. Chisum,[1,a)] Erich N. Grossman,[2] and Zoya Popović[1]

[1]*Department of Electrical and Computer Engineering, University of Colorado at Boulder, Boulder, Colorado 80309, USA*

[2]*Optoelectronics Division, National Institute of Standards and Technology, Boulder, Colorado 80305, USA*

This article describes the theory and design of an ultra-low noise electronic readout circuit for use with room temperature video-rate terahertz imaging arrays. First, the noise characteristics of various imaging detectors, including low resistance bolometers and high resistance diodes are discussed. Theoretical approaches to white and $1/f$ noise mitigation are examined, and a corresponding low-noise readout circuit is designed, built, and tested. It is shown that the circuit is capable of achieving detector limited noise performance for use in room temperature terahertz imaging systems. A thorough noise analysis of the circuit provides the necessary information for applying the readout circuit to any type of imaging detector, and more generally, any measurement of small signals from various source impedances in the presence of white and $1/f$ noise. W-band measurements of an 8-element, high-resistance detector array, and a 32-element, low-resistance detector array demonstrate the usefulness of the readout circuit. Finally, recommended circuit configurations for various detectors in the literature are provided, with theoretical performance metrics summarized. © *2011 American Institute of Physics*. [doi:10.1063/1.3599419]

I. INTRODUCTION

Millimeter-wave and terahertz imaging has been shown to be useful for concealed weapons detection through clothing,[1] low-visibility guidance,[2] and other applications.[3] The availability of sensitive detectors, such as bolometers and diodes makes passive imaging practical. The main challenges of passive terahertz imaging are a result of low signal and high noise levels at room temperature. Low signal-to-noise ratio (SNR) can be overcome with long integration times, but this makes video rate imaging[4] difficult. Presently, each imaging system requires a dedicated readout circuit,[5] but most terahertz imaging systems suffer from the same problems, and thus a general approach to detector readout is useful.

The goal of the first part of this paper is to present a general and comprehensive discussion on requirements of readout circuitry for room-temperature video-rate passive imaging. In order to increase the imaging speed, an array of detectors is used instead of a single, scanned detector. For this reason, the readout electronics consists of multiple channels of phase-sensitive low-noise amplifiers,[6,7] as illustrated in Fig. 1. Radiation from a blackbody target, characterized by temperature and emissivity, is modulated (at f_{mod}) through a mechanical chopper and received by an antenna-coupled detector array. The modulated nanovolt-level output of each detector is amplified and integrated prior to digitization. The remainder of the paper discusses the design and optimization of the readout electronics which accomplishes phase-sensitive amplification and signal integration of various arrayed detectors.

The two commonly available detectors from around 100 GHz to several THz are antenna-coupled resistive bolometers[8] and semiconductor diodes.[9] A bolometer

changes resistance as a function of temperature, which, in turn, changes due to varying incident RF power. In this work, bolometers are modeled as a voltage source with a low series resistance (hundreds of ohms[10]). Varying incident RF power on a diode is modeled as an induced current source with a high parallel resistance (tens of kilohms). These two equivalent circuits require different designs when optimizing a readout circuit for low-noise performance. Although the low-noise circuits discussed in this paper are developed for terahertz imaging arrays, the design principles are general and can be applied to any voltage measurement in the presence of white and $1/f$ noise.[11,12]

Section II of this paper discusses general noise theory as it applies to the analysis of the readout circuit, including quantification and reduction of detector thermal noise, and amplifier voltage and current noise in the low-frequency ($1/f$) and broadband regions of the spectrum. Section III describes a single amplifier channel, the basic building block of the readout electronics, including overall design considerations. This section concludes with an application of the noise theory developed in Sec. II to the specific readout circuit, and compares the theoretical noise performance with measured results, showing that it is important to identify constituent noise sources in the optimization of low-noise circuitry. Section IV describes two terahertz imaging array measurements, demonstrating the applicability of the readout electronics, and achieving detector limited noise performance.

II. ANALYSIS OF NOISE SOURCES

The dominant noise sources in this work are generated by the detector and by the electronics, and can generally be divided into white noise and $1/f$ noise. These noise sources have unique frequency distributions, and therefore useful quantities for describing noise are the *power* spectral
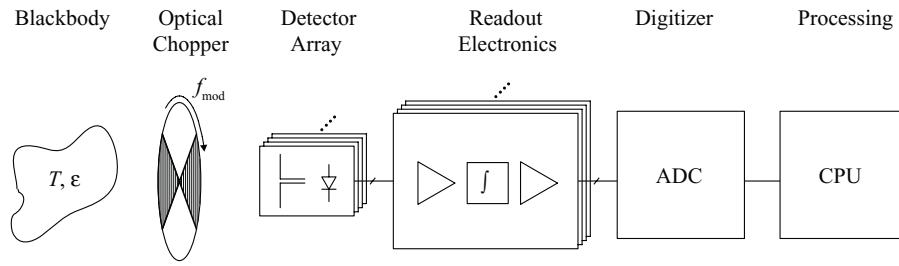

FIG. 1. Radiation from a blackbody target is modulated, detected, measured with a low-noise readout circuit, and digitized.

density, $S(f)$, expressed in V^2/Hz, and the *voltage* spectral density, $S_v(f)^{1/2}$, expressed in $V/\sqrt{Hz}$. Throughout this work, single-sided spectral densities are used. The variance, σ_v^2, often called the noise power of a zero mean signal in V^2, is calculated from the single-sided noise power spectral density as[13]

$$\sigma_v^2 = \int_0^\infty S(f)\mathrm{d}f. \tag{1}$$

The general class of linear circuits (filters, gain blocks, etc.) is described by their amplitude transfer functions in the frequency domain, $H(\jmath 2\pi f)$. In combination with the noise power spectral density, $S(f)$, the transfer of noise power from the input of a linear circuit block to its output is expressed as[14]

$$\sigma_{v\mathrm{nout}}^2 = \int_0^\infty S_{\mathrm{in}}(f)|H(\jmath 2\pi f)|^2\mathrm{d}f, \tag{2}$$

where $S_{\mathrm{in}}(f)$ includes the input-referred noise contribution of the network described by $H(\jmath 2\pi f)$.

White noise is characterized by a uniform power density across frequency (neglecting the quantum correction[15]), and is most commonly generated by a resistive material at temperatures above 0 K. Johnson[16] observed the lower limit on the mean-square voltage fluctuations of a measurement, due to a resistance R, with a noise bandwidth $f_2 - f_1$, at physical temperature T, is given as

$$\overline{V_{\mathrm{nth}}^2} = 4k_B T R(f_2 - f_1). \tag{3}$$

The root-means-square (rms) voltage can be expressed as the product of the thermal noise voltage spectral density, $S_{v\mathrm{nth}}^{1/2}$, and the square root of the equivalent noise bandwidth[17]

(ENBW):

$$\sigma_{v\mathrm{nth}} = S_{v\mathrm{nth}}^{1/2}\sqrt{\mathrm{ENBW}}, \tag{4}$$

where $S_{v\mathrm{nth}}^{1/2} = \sqrt{4k_B T R}$. In the case of a complex impedance, R is replaced by the real part of the complex impedance, $\mathrm{Re}(Z(f))$, and $S_{v\mathrm{nth}}^{1/2}$ becomes a function of frequency,[11] such that

$$\sigma_{v\mathrm{nth}} = \sqrt{4k_B T R \int_0^\infty \mathrm{Re}(Z(f))|H(\jmath 2\pi f)|^2\mathrm{d}f}. \tag{5}$$

In this work, a typical measurement consists of an ac-coupled detector with effective impedance, Z_s, a low-noise amplifier (LNA), and a feedback network, as shown in Fig. 2(a). The three dominant sources of *white* noise in this measurement are thermal voltage noise (v_{nth}), broadband amplifier voltage (v_{nBB}), and current (i_{nBB}) noise, as shown explicitly in Fig. 2(b). For convenience, current noise is converted to voltage noise as shown in Fig. 2(c).

The rms voltage due to broadband voltage noise from the amplifier is calculated as

$$\sigma_{v\mathrm{nBB}} = S_{v\mathrm{nBB}}^{1/2}\sqrt{\mathrm{ENBW}}. \tag{6}$$

The rms voltage due to broadband current noise from the amplifier depends on $Z_s(f)$, and is calculated as

$$\sigma_{i\mathrm{nBB}} = \sqrt{\int_0^\infty \left(\mathrm{Re}(Z_s(f))S_{i\mathrm{nBB}}^{1/2}\right)^2|H(\jmath 2\pi f)|^2\mathrm{d}f}. \tag{7}$$

The current noise through the feedback network and the thermal noise of the feedback network can be neglected if they are small compared to the input circuit and the detector, as shown in Fig. 2(c).

(a) Noisy components.   (b) Equivalent voltage and current sources.   (c) Equivalent voltage sources.
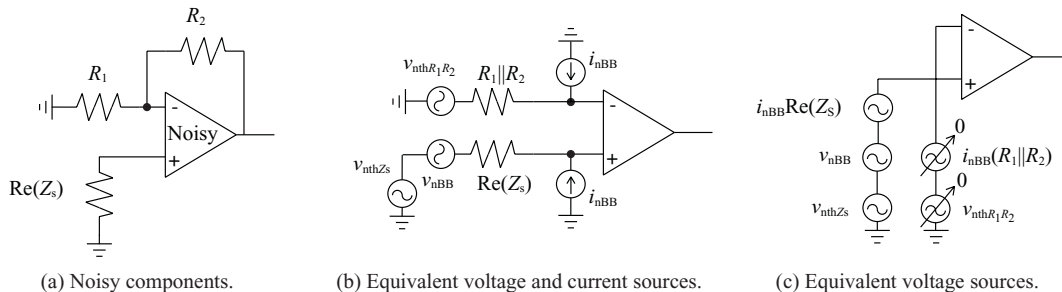
FIG. 2. A physical measurement is represented by noisy resistors and a noisy amplifier (a), or equivalently as noiseless components with explicit detector thermal noise ($v_{\mathrm{nth}Zs}$), feedback thermal noise ($v_{\mathrm{nth}R1R2}$), op-amp voltage noise (v_{nBB}), and op-amp current noise (i_{nBB}) (b). Finally, noise sources can be represented as simplified equivalent voltage sources (c).
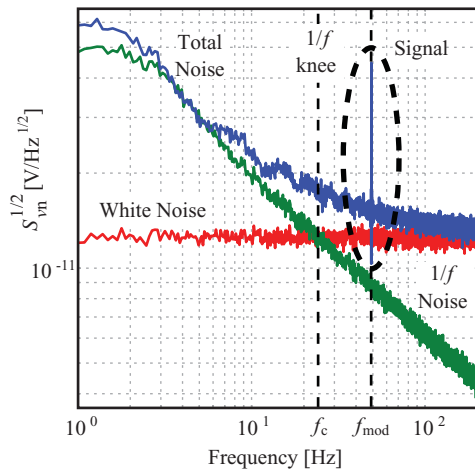
FIG. 3. (Color online) A simulated low power signal at f_{mod} is buried in white and $1/f$ noise. Phase sensitive detection can extract the modulated signal from the noise with the required SNR, while low-pass filtering yields diminishing returns for increased integration time.

The physical mechanisms behind $1/f$ noise are not well understood, but are universally characterized by a power spectral density proportional to $1/f$. In this work, we are concerned with flicker noise generated in a biased detector[18] and in the front-end of an amplifier.[7]

Uncorrelated noise power adds in quadrature,

$$\sigma_{v\text{tot}} = \sqrt{\sigma_{v1}^2 + \sigma_{v2}^2}, \tag{8}$$

so that one noise source will usually dominate the total measurement noise. The crossover point at which, for example, $1/f$ noise-dominance yields to white noise-dominance is called the $1/f$ knee, designated f_c in Fig. 3.

A. Noise reduction

The overall noise performance of a properly designed room-temperature imaging system is dominated by detector noise, not readout noise. Here, we explore techniques for reducing uncertainty in the final measurement due to noise in the readout electronics.

The source resistance of a room-temperature detector is optimized for best performance[9,10,19,20] so, referring to Eq. (3), the primary method of thermal noise reduction in this work is the reduction of measurement bandwidth. In 1979, Grimbleby described the "ideal averaging filter"[21] (IAF) as the most efficient method for white noise reduction in the measurement of a constant signal. The IAF integrates (filters) a noisy signal for a period of time, τ_{int}, during which the signal grows linearly and the noise grows as the square root of integration time. Thus, SNR increases as the square root of integration time. It is necessary that each IAF measurement be independent of previous measurements and the time-domain step-response be linear.

The "gated integrator" shown in the dashed box of Fig. 4 approximates the ideal averaging filter.[13] The single-pole low-pass filter has an exponential integration response; however, when $\tau_{\text{int}} \ll RC$, it is approximately linear. The gated integrator clears the previous signal, integrates for τ_{int}, and holds the
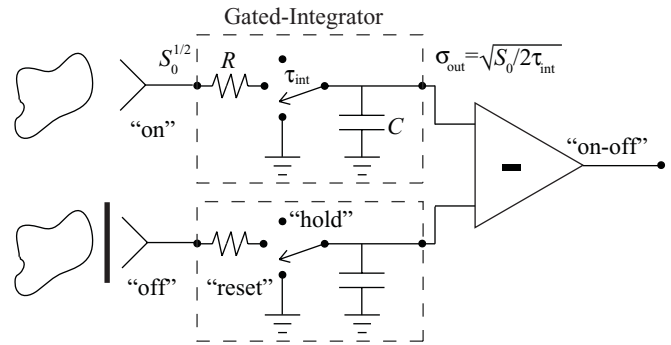

FIG. 4. The "on-off" measurement topology, for the reduction of white noise and $1/f$ noise is the difference of two subsequent "on" measurement protocols, one with the signal nulled. The gated-integrator is shown in the dashed box.

signal for sampling and digitization. We refer to this white-noise reducing measurement technique as the "on" measurement protocol. The rms voltage at the output of an "on" measurement is $\sigma = \sqrt{S_0/2\tau_{\text{int}}}$, in the presence of white noise only. However, in the presence of $1/f$ noise, fluctuations are divergent and a different technique is needed.

Figure 3 shows the frequency domain voltage spectral density, $S_v(f)^{1/2}$, of a small signal, periodic at f_{mod}, in the presence of seemingly overwhelming white and $1/f$ noise. The signal is stronger than the white noise and $1/f$ noise at f_{mod}, so by applying appropriate filtering the modulated signal can be extracted. For $\sqrt{\tau_{\text{int}}}$ improvement in SNR, filter integration must be coherent and thus f_{mod} should be greater than f_c. This work attempts to measure a dc signal so it must be intentionally modulated. This type of measurement is referred to as phase sensitive detection[6] (PSD).

A realization of PSD is the "on-off" measurement protocol, depicted in Fig. 4, consisting of two measurements taken every $1/f_{\text{mod}}$ seconds, synchronous with the modulated signal. The measurement in the first half-period, $\tau_{\text{int}} = 1/2f_{\text{mod}}$, is taken according to the "on" measurement protocol to reduce white noise. For the remaining half-period a similar measurement with the signal nulled is conducted, and is referred to as the "off" measurement. The difference of the two measured voltages constitutes the "on-off" measurement protocol, which removes any $1/f$ drift below f_{mod}.

B. Measurement protocol comparison

The mean-square fluctuation of a sampled voltage, at the output of an analog circuit is calculated as[13]

$$\sigma^2 = \int_0^\infty S(f)\,|W(\jmath 2\pi f)|^2\,\mathrm{d}f, \tag{9}$$

where $S(f)$ is the power spectrum of the input noise and $W(\jmath 2\pi f)$ is the measurement protocol transfer function. Table I summarizes the results of Eq. (9) for the "on" and "on-off" measurement protocols in the presence of white ($S = S_0$) and $1/f$ ($S = S_0 f_c/f$) noise. The white-noise variance of the "on" measurement (averaging for τ_{int}) is inversely proportional to integration time; however, the $1/f$-noise variance diverges with integration time. The variance of the "on-off"

TABLE I. Output variation of an "on" measurement protocol diverges in the presence of $1/f$ noise, while an "on-off" measurement protocol maintains $1/f$ noise to a constant low level. $\omega = 2\pi f$ and τ is the integration time.

	σ^2 "on" [V^2]	σ^2 "on-off" [V^2]
$w(t)$	$\dfrac{1}{\tau}\mathrm{rect}\left(\dfrac{t-\frac{\tau}{2}}{\tau}\right)$	$\dfrac{2}{\tau}\mathrm{rect}\left(\dfrac{t-\frac{\tau}{4}}{\frac{\tau}{2}}\right) - \dfrac{2}{\tau}\mathrm{rect}\left(\dfrac{t-\frac{3\tau}{4}}{\frac{\tau}{2}}\right)$
$W(J\omega)$	$e^{-J\omega\frac{\tau}{2}}\dfrac{\sin(\omega\tau/2)}{\omega\tau/2}$	$2Je^{-J\omega\frac{\tau}{2}}\dfrac{\sin^2(\omega\tau/4)}{\omega\tau/4}$
White	$\dfrac{S_0}{2\tau}$ (Ref. [21])	$\dfrac{2S_0}{\tau}$
$1/f$	divergent	$4\ln 2 S_0 f_c$ (Ref. [13])

measurement also reduces the white-noise variance (though variance is four times higher than the "on" measurement) and maintains the $1/f$-noise variance at a constant level. This is the preferred measurement protocol for this work. A similar technique was pioneered in the original Dicke radiometer,[22] and is often used for bolometric radiometry measurements.[8]

III. READOUT SINGLE CHANNEL DESIGN

The readout electronics are designed to interface with an array of detectors, so the complete readout is a parallelized array of digitally sampled channels. Each channel should accurately measure detector noise, which requires channel noise to be lower than detector noise. Section II indicates that detector limited noise performance can be achieved through the proper application of a gated integrator employed in an "on-off" measurement protocol.

The front-end and back-end of such a measurement are shown in Figs. 5(a) and 5(b), respectively. The front-end amplifies the detector signal and applies a variable ENBW limit ($1/2\tau_{\mathrm{int}}$) through the programmable gated integrator. The back-end buffers the gated integrator and performs additional amplification. A conceptual noise analysis provides further insight into the circuit parameters critical to the detector limited performance (e.g., gain, ENBW).

If the equivalent input noise spectral density, $S_{v\mathrm{nin}}^{1/2}$, in Fig. 5(a) is assumed constant over frequency, and the "on-off"
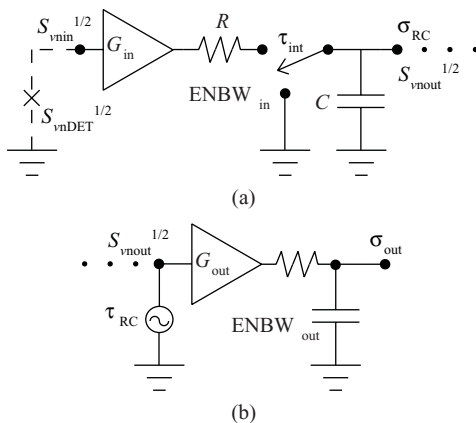

(a)

(b)

FIG. 5. The front-end of a single readout channel (a) amplifies and integrates the input signal and noise. The back-end of the channel provides buffering and additional gain (b).

measurement protocol is appropriately applied ($f_{\mathrm{mod}} > f_c$), a simplified noise analysis need only consider constant white noise sources (Fig. 2(b)).

The analysis proceeds as follows: (1) determine noise at the output of the gated integrator, σ_{RC}, due to the front-end (Fig. 5(a)) as a function of the programmable integration time, τ_{int}, (2) determine noise at the output of the channel, σ_{out}, due to the back-end (Fig. 5(b)), and (3) incoherently combine the two.

The noise at the output of the gated integrator due to front-end noise sources, according to Eq. (6), is

$$\sigma_{RC} = S_{v\mathrm{nin}}^{1/2} G_{\mathrm{in}} \frac{\tau_{\mathrm{int}}}{RC}\sqrt{\mathrm{ENBW}_{\mathrm{in}}} \quad \text{or} \tag{10}$$

$$\sigma_{RC} = \frac{S_{v\mathrm{nin}}^{1/2} G_{\mathrm{in}}}{RC}\sqrt{\frac{\tau_{\mathrm{int}}}{2}}, \tag{11}$$

where $S_{v\mathrm{nin}}^{1/2}$ is the combined contribution of the voltage and current noise of the front-end amplifier. From Eq. (8), the total readout channel noise is

$$\sigma_{\mathrm{out}} = \sqrt{\underbrace{(\sigma_{RC}G_{\mathrm{out}})^2}_{\text{Front-end}} + \underbrace{\left(S_{v\mathrm{nout}}^{1/2}G_{\mathrm{out}}\sqrt{\mathrm{ENBW}_{\mathrm{out}}}\right)^2}_{\text{Back-end}}}. \tag{12}$$

Similarly, the noise of the final digitized data is the incoherent addition of the output of the readout electronics, σ_{out}, and the digitizer noise floor, σ_{DAQ}:

$$\sigma_{\mathrm{fin}} = \sqrt{\sigma_{\mathrm{out}}^2 + \sigma_{\mathrm{DAQ}}^2}. \tag{13}$$

As long as the first term in Eq. (13) dominates the second, the measurement will be dominated by the noise of the readout electronics and not the digitizer. If the first term in Eq. (12) dominates, Eq. (13) simplifies to

$$\sigma_{\mathrm{fin}} \approx \frac{S_{v\mathrm{nin}}^{1/2}G_{\mathrm{in}}G_{\mathrm{out}}}{RC}\sqrt{\frac{\tau_{\mathrm{int}}}{2}}, \tag{14}$$

which is just the front-end noise amplified by G_{out}, as expected for the front-end noise dominance. The noise spectral density of the front-end electronics and the detector are both limited by the same ENBW (i.e., of the gated integrator), so as long as $S_{v\mathrm{nin}}^{1/2}$ is less than the detector noise spectrum, the entire measurement is detector limited.

The practical realization of the circuit in Fig. 5 must take into account (1) the high input gain, G_{in}, required for low-level terahertz signals, and (2) the frequency dependence of the coupled detector impedance, $Z_s(f)$. The high gain (G_{in} up to 100 000) is accomplished through multiple cascaded gain stages, each of which must be bandwidth limited so that they do not saturate by amplified front-end noise. The frequency dependence of $Z_s(f)$ is accounted for by integrating over frequency. The realized circuit is shown in Fig. 6 with pertinent parameters listed in Table II.

The predicted noise is shown in Fig. 7 for the circuit with two different LNAs, the AD797 and the OPA124 (trade names are provided for technical clarity and do not imply endorsement by NIST). Detector thermal noise, $\sigma_{v\mathrm{nthZs}}$, LNA voltage noise, $\sigma_{v\mathrm{nBB}}$, and LNA current noise, $\sigma_{i\mathrm{nBB}}$, are shown
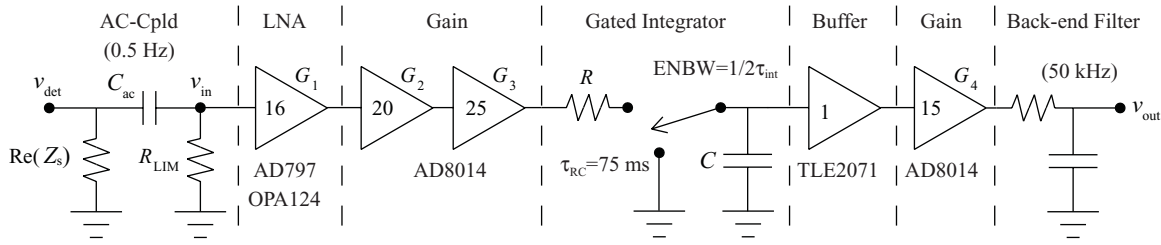
FIG. 6. A single low-noise electronic readout channel is shown in simplified schematic. Table II summarizes the important specifications for each amplifier. The AD797/OPA124 is a low-noise amplifier, the AD8014 is a general purpose amplifier, and the TLE2071 is a low bias current buffer for the integrator.

as constituents of the total theoretical noise, σ_{fin}. The gray region, where $\sigma_{v\text{nth}Zs}$ is dominant, indicates detector limited noise performance. For $\text{Re}(Z_s) < 100$, constant voltage noise from both LNAs dominates noise performance. As $\text{Re}(Z_s)$ increases, detector Johnson noise dominates the LNA voltage noise, first for the AD797, and then for the OPA124. For high $\text{Re}(Z_s)$, the AD797 current noise dominates, while the OPA124 remains in the detector limited regime, but with a roll-off due to the parallel R_{LIM} in the ac coupling filter, as shown in Fig. 6. The roll-off will shunt signal from the detector in larger proportion than the noise is reduced, so R_{LIM} and C_{ac} should be adjusted for specific detector impedances, to be discussed in Sec. IV.

In summary, this section has presented the design of a detector limited readout channel. The results useful for measurement applications are given in Fig. 7 with the following conclusions:

1. For $(100 < \text{Re}(Z_s) < 6\,\text{k}\Omega)$, such as bolometric detectors,[10] the AD797 is detector limited and should be used because of its overall lower noise at low resistances.
2. For $(\text{Re}(Z_s) < 2\,\text{k}\Omega)$, such as diode detectors,[9,23] the OPA124 is detector limited; but, the input circuit should be set to prevent shunted signal.

IV. EXAMPLE TERAHERTZ IMAGING MEASUREMENTS

The detector limited readout channel described in Sec. III is parallelized for terahertz imaging array measurements. Figure 1 shows the measurement procedure starting with a mechanical chopper which provides the modulation (f_{mod}) of blackbody radiation. A video-rate of 30 fps allows each channel a maximum integration time of $\tau_{\text{int}} = 1/(2 \times 30\,\text{fps})$ = 16.5 ms/frame for the "on" and the "off" half-period. The digitizer records each of the channel voltages sequentially, once per "on" and "off" state. Finally, the central processing

TABLE II. OP-AMP Specifications.

Spec	AD797	OPA124	AD8014	TLE2071
BW (MHz)	8	1.5	400	10
$S_{vn\text{BB}}$ (nV/$\sqrt{\text{Hz}}$)	1.3	6	3.5	11–17
$S_{in\text{BB}}$ (pA/$\sqrt{\text{Hz}}$)	3	0.0005	5	0.0028
$f_{c1/f}$ (Hz)	10	220	…	160
I_{bias} (nA)	250	0.001	5000	0.015
V_{off} (mV)	0.025	0.2	2.5	0.34–4

unit performs the PSD algorithm. Additional averaging or other signal processing can be performed at the expense of frame update rate.

Each element in the detector array is an antenna-coupled power detector, characterized by dynamic resistance, R_{dyn}, and intrinsic current responsivity, $\mathfrak{R}_I$, which are calculated from a Taylor expansion of the dc *IV*-curves as[20,24]

$$R_{\text{dyn}} = \frac{dV}{dI}\ [\Omega]\ \text{and} \tag{15}$$

$$\mathfrak{R}_I = \frac{d^2I/dV^2}{2dI/dV}\ [\text{A/W}]. \tag{16}$$

The zero-bias dynamic resistance, R_{zb}, is used to predict detector white noise, while responsivity is a measure of the signal from the device. The intrinsic voltage responsivity is calculated as

$$\mathfrak{R}_V = \mathfrak{R}_I R_{\text{zb}}\ [\text{V/W}]. \tag{17}$$

A total system thermal responsivity can be calculated from measured parameters as

$$\mathfrak{R}_T = \frac{\Delta V_{\text{out}}/G_{\text{tot}}}{\Delta T_{\text{bb}}} = \frac{\Delta V_{\text{det}}}{\Delta T_{\text{bb}}}\ [\text{V/K}], \tag{18}$$

where ΔT_{bb} is the radiometric temperature difference between two blackbody targets, G_{tot} is the readout gain, ΔV_{out} is the measured voltage difference at the output of the readout due to ΔT_{bb}, and ΔV_{det} is the measured voltage difference referred to the detector. This measurement includes coupling, mismatch, and other efficiencies between an ideal blackbody and the output of the readout.

A standard measure of performance which includes responsivity and noise is the noise equivalent temperature difference (NETD), usually normalized to video rate (30 Hz):

$$\text{NETD} = \frac{\text{NEP}}{k_{\text{B}}\Delta f}\sqrt{\frac{1}{2 \times 33\text{ms}}}\ [\text{K}]. \tag{19}$$

NETD can be calculated directly from the measured, input-referred noise (σ_{in}) and thermal responsivity ($\mathfrak{R}_T$):

$$\text{NETD} = \frac{S_v^{1/2}\sqrt{\frac{1}{2\times0.033}}}{\mathfrak{R}_T} = \frac{\sigma_{\text{in}}}{\mathfrak{R}_T}, \tag{20}$$

where σ_{in} and $\mathfrak{R}_T$ are referred to a 33 ms integration time.

Measurements with the readout circuit from Fig. 6 were performed for two terahertz imaging systems: (1) an

FIG. 7. (Color online) Detector thermal noise (σ_{vnthZs}), amplifier voltage (σ_{vnBB}), and current noise (σ_{inBB}) add in quadrature for the total theoretical noise (dashed, diamond) showing good agreement with measured total noise (solid, circle). The gray regions indicate ideal operating regions in the "σ_{vnthZs} limit." The AD797 is ideal for low resistance detectors and the OPA124 for high resistance detectors.

8-element, horn-antenna coupled diode array similar to Ref. 19 available at NIST-Boulder, and (2) a 32-element array of horn-antenna coupled diodes located at the Army Research Laboratory (ARL) in Adelphi, MD.[25]

A. System 1: High Re(Z_{det})

Figure 8 shows a photograph of the 8-element terahertz imaging array at NIST-Boulder employing ErAs/InAlGaAs diode detectors.[19] The diodes were initially characterized with dc *IV*-curve measurements for noise and responsivity predictions. As a result of multiple fabrication runs, the diodes exhibit significant non-uniformity. At the time of these measurements, diodes 1, 4, and 8 were no longer functional, and diode 2 had poor performance. Neglecting these diodes, the typical zero-bias resistance is 20 kΩ, with voltage responsivity of ∼3 nV/K, yielding an expected NETD between 20 and 30 K. Table III summarizes the results of the *IV*-curve characterization.

The readout was originally configured for use with a 500 Ω bolometric detector[10] so the ac-coupling input filter included a 4.2 kΩ shunt resistor (R_{LIM}). Using this default configuration, the measured input-referred noise (with

an OPA124) for a typical diode, with a measurement gain of 14 750, is ∼510 μV/14 750 = 35 nV, as shown for diode 5 in Fig. 9. In a 10 ms integration time, that is 35 nV/$\sqrt{(1/(2 \times 10 \text{ ms}))}$ = 5 nV/$\sqrt{\text{Hz}}$, which is close to the 5.7 nV/$\sqrt{\text{Hz}}$ expected for an effective resistance of 2 kΩ (20 kΩ detector in parallel with the input circuit).

To measure $\Re_T$ directly, a mechanical chopper is placed in front of the diode detector array. Quadrants of the chopper wheel present alternate hot (295 K Eccosorb®) and cold (77 K liquid nitrogen) loads to the diode array. The input referred response is typically 220 μV/14 750 = 14.9 nV, and maximally 277 μV/14750 = 18.8 nV, as shown in Fig. 10. From Eq. (18), the input-referred thermal responsivity is $\Re_T$ = 18.8 nV/218 K = 86 pV/K. The NETD, from Eq. (20) is 226 K which is significantly higher than expected. Given the practical considerations discussed in Sec. III of interfacing with a specific detector resistance, if the 4.2 kΩ shunt resistor in the input circuit is replaced with a larger resistor (e.g., 1 MΩ (Ref. 26)), the predicted coupled responsivity increases by a factor of 10.5. Remeasuring noise with this input impedance, and including an optical coupling efficiency of ∼30%, as discussed in detail in Ref. 25, we obtain the expected 29 K NETD from Table III, which confirms that the
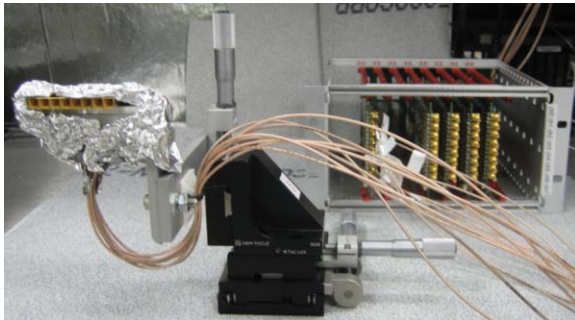

FIG. 8. (Color online) An 8-element antenna-coupled, zero-bias diode imaging array is shielded to reduce interference. A chassis hosts up to eight, 8-channel readout boards.

TABLE III. System 1 array characterization from dc *IV*-curves provides zero-bias resistance (R_{zb}), current responsivity ($\Re_I$), and voltage responsivity ($\Re_V$) from Eqs. (15)–(17). Equation (20) gives antenna mismatch responsivity ($\Re_V(1 - |S_{11}|^2)$), thermal responsivity ($\Re_T$), and NETD for a RF bandwidth of 10 GHz and a 33 ms post-detection integration time.

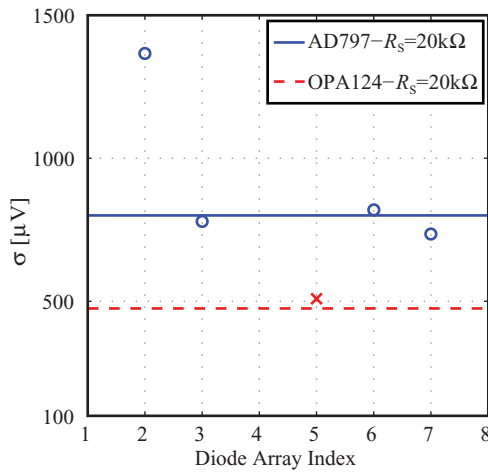| Diode	1	2	3	4	5	6	7	8
R_{zb} [kΩ]	…	12.1	21	…	28.6	20.3	20.4	…
$\Re_I$ [A/W]	…	5.7	14.5	…	13.5	14.7	14.7	…
$\Re_V$ [kV/W]	…	69	300	…	390	300	300	…
$\Re_V(1 - |S_{11}|^2)$ [kV/W]	…	8.5	22	…	21	23	23	…
$\Re_T$ [nV/K]	…	1.2	3	…	2.9	3.1	3.1	…
NETD$_{33 \text{ ms},10 \text{ GHz}}$ [K]	…	47	23	…	29	23	23	…

FIG. 9. (Color online) Measured noise for diodes 3, 6, and 7 agrees with theory with an AD797 LNA. Diode 5 agrees with theory with an OPA124. Horizontal lines indicate the measured noise with a 20 kΩ shielded resistor. Note that diode 2 has anomalously high noise (as expected due to low resistance and responsivity from IV-curves), and diodes 1, 4, and 8 were damaged.
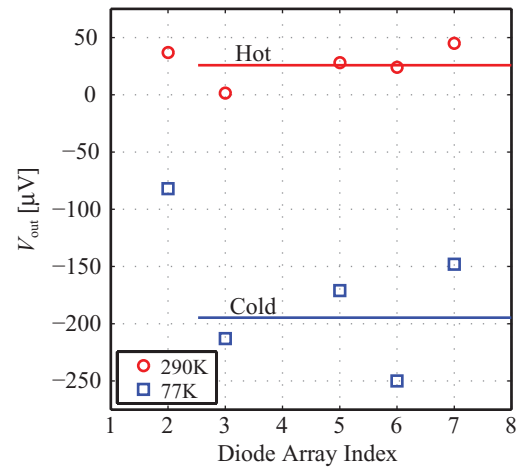

FIG. 10. (Color online) The typical response of each diode from the "hot" to "cold" state, at the output of the readout circuit, in a 10 ms integration is ~220 μV. Diode 2 has anomalously low signal and diodes 1, 4, and 8 were damaged.

increased NETD is completely attributed to the shunted signal when using $R_{\text{LIM}} = 4.2\,\text{k}\Omega$, and not excess noise. Thus, the recommended configuration for optimal noise, and responsivity for these diodes is $R_{\text{LIM}} \approx 1\,\text{M}\Omega$ with the OPA124.

B. System 2: Low Re(Z_{det})

The readout circuit described in this work was also sent to ARL for independent measurement with a 32 element array of Sb-based backward tunnel diodes.[25] The Re(Z_{det}) was 2 kΩ (Ref. 9), much lower than for the system measured at

NIST-Boulder. R_{LIM} was set to 6.8 kΩ to maximize the signal, and the AD797 was used as the LNA. Measured NETDs across the array of diodes were reported to be typically 40 K, with ranges from 20–80 K which were deemed too high to be useful by a factor of four.[25] However, it was noted that degraded NETD was primarily due to excessive interference which is reduced in system 1 by shielding as seen in Fig. 8. Using the responsivity of 2.2 nV/K from Ref. 25, and the noise performance of a shielded 2 kΩ detector of 5 nV/$\sqrt{\text{Hz}}$ (as demonstrated in Fig. 7), we expect a NETD of 8.8 K. However, without proper shielding and careful grounding this NETD rises significantly, underscoring the importance of shielding in order to achieve the theoretical detector limited performance of the readout circuit.

TABLE IV. Zero-bias resistance (R_{zb}), input circuit shunt resistance (R_{LIM}), and LNA selection for each detector determine an expected responsivity ($\mathfrak{R}_T$) and NETD.

	Recommended config.			Measurements[a]			Limit
	R_{zb} [Ω]	LNA	R_{lim} [Ω]	$S_{vn}^{1/2}$ [nV/$\sqrt{\text{Hz}}$]	$\mathfrak{R}_T$ [nV/K]	NETD [K]	NETD [K]
System 1 - Sec. IV A	28 k	OP124	4.2 k	5	.086	226	29
System 1 - input matched	28 k	OP124	1 M	21	0.9	89	29
System 2 - Section IV B (Ref. 25)	2 k	AD797	6.8 k	22	2.2	40	2.2
System 2 - no interference	2 k	AD797	6.8 k	5	2.2	8.8	2.2
Nb Bolometer (Ref. 10)	505	AD797	4.2 k	2.9	0.7[b]	16	...
Hetero[c] diode (Ref. 27)	860	AD797	4.2 k	2.4[d]	0.6[d]	24	11
Hetero diode (Ref. 23)	6.5 k	OP124	1 M	10.3	2.3[e]	17	...
Sb diode (Ref. 28)	18 k	OP124	1 M	17	3.9[f]	17	...
Similar to this work (Ref. 23)	20 k	OP124	1 M	18	2.5[g]	28	...
Hetero diode (Ref. 19)	955 k	OP124	2 M	125	3.5[h]	9.7	2.47

[a]Results are based upon measurements in this work for the two systems discussed, while italicized entries are calculated for various systems based upon results in the literature.
[b]Reference 10 shows $\beta = 53$V/W at $I_{\text{bias}} = 200\mu$A. $\Delta f_{\text{RF}} = 1$THz (Ref. 1).
[c]"Hetero" refers to ErAs-InGaAlAs hetero-junction diodes (noted in corresponding references).
[d]Reference 27 shows NEP = 2 pW/$\sqrt{\text{Hz}}$, and $\mathfrak{R}_V = 1200$ V/W, and assuming $\Delta f_{\text{RF}} = 35$ GHz.
[e]Reference 23 shows $\mathfrak{R}_I = 11.7$ A/W. The horn antenna has ~$\Delta f_{\text{RF}} = 10$GHz, with an impedance of 400 Ω. After mismatch loss, $\mathfrak{R}_T = 2.3$nV/K.
[f]Reference 28 shows $\mathfrak{R}_V = 3687$ V/W, including 50 Ω mismatch. In the same 400 Ω antenna as Ref. 19, $\mathfrak{R}_V = 333,000$ V/W, or $\mathfrak{R}_T = 3.9$ nV/K, if $\Delta f_{\text{RF}} = 10$GHz.
[g]Reference 23 shows $\mathfrak{R}_I = 11.7$ A/W. The horn antenna has ~$\Delta f_{\text{RF}} = 10$GHz, with an impedance of 400 Ω. After mismatch loss, $\mathfrak{R}_T = 2.5$nV/K.
[h]Figure 6 of Ref. 19 shows $\mathfrak{R}_T = 50$ nV/K. Assuming thermal noise of detector is dominant, NETD = 9.7 K.
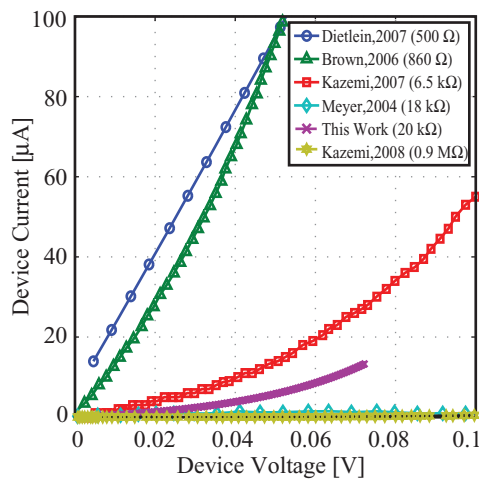
FIG. 11. (Color online) Device *IV*-curves are used to predict zero-bias dynamic resistance which determines how the readout input circuit should be configured (R_{LIM} and LNA). Devices references are as noted for trace markers: circle (see Ref. 10), triangle (see Ref. 27), square (see Ref. 23), diamond (see Ref. 28), cross (This Work), hexagram (see Ref. 19).

V. CONCLUSION

The measurements from Sec. IV show the applicability of the readout circuit to various imaging systems. Correctly configured, this circuit can achieve detector limited performance with any direct detector at terahertz, or other frequencies. Recommended configurations for various detectors published in the literature are based on detector *IV*-curves, as shown in Fig. 11, and are summarized in Table IV. The zero-bias dynamic resistance, R_{zb}, is calculated from the *IV*-curve and motivates selection of the LNA based on the detector limited regions defined in Fig. 7. R_{LIM} is selected to simultaneously prevent the LNA bias current from saturating the circuit, and from shunting too much of the detector signal to ground, while still enforcing a low-frequency cutoff of ~0.5 Hz. Figure 11 shows the published *IV*-curves for various detectors in the literature,[10,19,27,28] with R_{zb} ranging from 500 Ω to almost 1 MΩ. The recommended readout configuration for each detector is given in Table IV.

The main contribution of this paper is a flexible readout circuit design, made with off-the-shelf components that can be easily adapted to any direct detector for achieving detector limited noise performance for video-rate arrays. Recommendations are provided for maximizing the coupled responsivity of any diode based on a dc *IV*-curve characterization. The approach is demonstrated on arrays of up to 64 detectors, but is scalable to imaging systems with much larger arrays.

ACKNOWLEDGMENTS

[1] E. N. Grossman, C. R. Dietlein, J. Chisum, A. Luukanen, J. E. Bjarnasson, and E. R. Brown, in *Passive Millimeter-Wave Imaging Technology X*, edited by R. Appleby and D. A. Wikner (SPIE, Orlando, FL, USA, 2007), Vol. 6548, pp. 654807–8.

[2] R. Appleby, P. Coward, and J. N. Sanders-Reed, *Proceedings of Passive Millimeter-Wave Imaging Technology XII*, Proc. of SPIE, vol. 7309, pp. 73090A (SPIE, Orlando, FL, USA, 2009).

[3] P. Siegel, IEEE Trans. Microwave Theory Tech. **50**, 910 (2002), ISSN 0018-9480.

[4] A. Luukanen, L. Gronberg, P. Helisto, J. S. Penttila, H. Seppa, H. Sipola, C. R. Dietlein, and E. N. Grossman, *Passive Millimeter-Wave Imaging Technology X*, Proc. of SPIE, vol. 6548 (SPIE, Orlando, FL, USA, 2007).

[5] A. Luukanen, E. N. Grossman, A. J. Miller, P. Helisto, J. S. Penttila, H. Sipola, and H. Seppa, IEEE Microw. Wirel. Compon. Lett. **16**, 464 (2006).

[6] D. P. Blair and P. H. Sydenham, J. Phys. E **8**, 621 (1975).

[7] G. Erdi, IEEE J. Solid-State Circuits **SC-16**, 653 (1981).

[8] P. L. Richards, J. Appl. Phys. **76**, 1 (1994).

[9] J. Schulman and D. Chow, IEEE Electron Device Lett. **21**, 353 (2000), ISSN 0741-3106.

[10] C. Dietlein, J. Chisum, M. Ramirez, A. Luukanen, E. Grossman, and Z. Popović, in *IEEE/MTT-S International Microwave Symposium Digest, 2007* (IEEE, Honolulu, HI, USA, 2007), pp. 1165–1168, ISBN 0149-645X.

[11] H. B. Callen and T. A. Welton, Phys. Rev. **83**, 34 (1951).

[12] P. Helisto and H. Seppa, IEEE Trans. Instrum. Meas. **50**, 453 (2001), ISSN 0018-9456.

[13] D. R. White and J. F. Clare, Meas. Sci. Technol. **3**, 1 (1992).

[14] W. B. Davenport and W. L. Root, *An Introduction to the Theory of Random Signals and Noise* (IEEE, New York,1987), ISBN 0-87942-235-1.

[15] B. Oliver, IEEE Proc. **53**, 436 (1965), ISSN 0018-9219.

[16] J. B. Johnson, Phys. Rev. **32**, 97 (1928).

[17] P. Kittel, Rev. Sci. Instrum. **48**, 1214 (1977), ISSN 00346748.

[18] A. C. Young, J. D. Zimmerman, E. R. Brown, and A. C. Gossard, Appl. Phys. Lett. **88**, 073518 (2006), ISSN 00036951.

[19] H. Kazemi, C. Nguyen, B. Brar, G. Rebeiz, G. Nagy, L. Tran, A. Young, and E. Brown, in *IEEE/MTT-S International Microwave Symposium Digest, 2008* (IEEE, Atlanta, GA, USA, 2008), pp. 297–300, ISBN 0149-645X.

[20] J. D. Zimmerman, E. R. Brown, and A. C. Gossard, J. Vac. Sci. Technol. B **23**, 1929 (2005), ISSN 0734211X.

[21] J. B. Grimbleby, Radio Electron. Eng. **49**, 530 (1979).

[22] R. H. Dicke, Rev. Sci. Instrum. **17**, 268 (1946), ISSN 00346748.

[23] H. Kazemi, G. Nagy, L. Tran, E. Grossman, E. Brown, A. Gossard, G. Boreman, B. Lail, A. Young, and J. Zimmerman, in *IEEE/MTT-S International Microwave Symposium Digest, 2007* (IEEE, Honolulu, Hl, USA, 2007), pp. 1367–1370, ISBN 0149-645X.

[24] H. C. Torrey and C. A. Whitmer, *Crystal Rectifiers*, in MIT Radiation Laboratory Series, Vol. 15 (McGraw, New York, 1948).

[25] D. Wikner and E. Grossman, *Passive Millimeter-Wave Imaging Technology XII*, Proc. of SPIE, vol. 7309, pp. 730909, (SPIE, Orlando, FL, USA, 2009).

[26] The extremely low bias current of the OPA124 allows for very large R_{LIM} without saturating the circuit.

[27] E. R. Brown, H. Kazemi, A. C. Young, J. D. Zimmerman, T. L. J. Wilkinson, J. E. Bjarnason, J. B. Hacker and A. C. Gossard, Proc. SPIE vol. 6212, pp. 62120S (SPIE, Orlando, FL, USA, 2006).

[28] R. Meyers, P. Fay, J. Schulman, S. Thomas, D. Chow, J. Zinck, Y. Boegeman, and P. Deelman, IEEE Electron Device Lett. **25**, 4 (2004), ISSN 0741-3106.